

RoboBoat 2025: VantTec Technical Design Report

VTec S-IV

Max Pacheco, Christian Villarreal, Emiliano Munguía, Demian Marín Martínez, and David Emmanuel Güemes
Tecnologico de Monterrey
School of Sciences and Engineering
Monterrey, Mexico

Abstract—This report presents the competition, design, and testing strategies implemented by our team for the 2025 RoboBoat competition with our VTEC-S-IV vehicle. Building on the lessons learned from our boat's performance in the previous year's competition, we tackled a thorough redesign with a main focus on modularity and adaptability to solve diverse competition tasks.

Our design strategy emphasized a modular system for rapid and straightforward configuration and integration of subsystems. A testing strategy was central to the redesign process, combining simulation validation and real-world testing to improve and verify subsystem functionality and performance. Test plans and results demonstrated functional task completion, system reliability and ease of deployment.

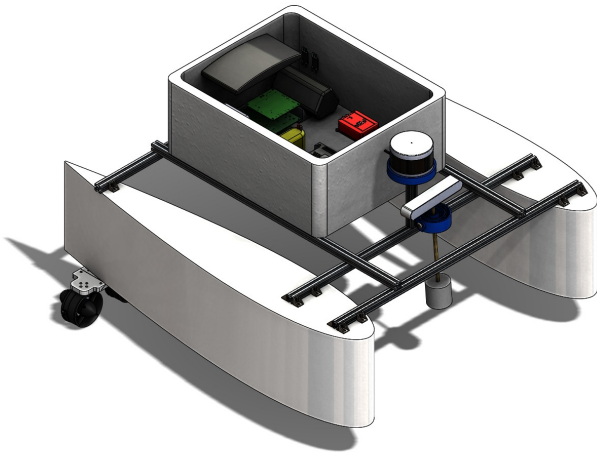


Fig. 1. VTec S-IV Final Hull Iteration.

I. COMPETITION STRATEGY

VantTec's strategic vision for RoboBoat 2025's Autonomy Challenge is to successfully complete all tasks with maximum scoring on finals, prioritizing time management for extra bonus points. To accomplish this goal, reflecting on our last boat iteration, major changes were needed: in mechanics, an easy and modular mechanism attachment approach, new and modular hulls for the catamaran, a more powerful propulsion system, and an easier-to-access electronics box for any component replacements, last-minute changes, or rearrangements; in electronics, a new modular PCB for mechanisms considering general commonly used output for motor control in the team,

like H-Bridge, NEMA drivers, and 5 V output from level shifters; finally, in software, a subsystem validation message to guarantee all the time the needed nodes are running and external components are connected, a way to run all tasks' state machines from the same node based on a scheduler, a new method to detect and classify objects using a sensor fusion of LiDAR and camera, adaptations for new tasks, more reliable localization algorithms and tools, among other changes.

A. Trade-offs between Complexity and Reliability

After RoboBoat 2024, we knew we wanted to change a lot of things in all areas. We decided to take risks and make big changes. We designed a new hull, using a new custom control scheme, new mechanisms PCB was built, and tried new methods for object detection with LiDAR. We were confident that in this year we were going to be able to achieve our goals given our current team.

B. Course Approach

Following our strategic vision, in order to maximize scoring, all 6 missions must be completed in the least amount of time. As a result, all tasks are attempted sequentially, except for Task #5, which can potentially be addressed while solving the other tasks, although not necessarily. Furthermore, the general course approach is to start with a preliminary task schedule. The schedule is set in a configuration file, so the boat knows whether to stop after completing a mission, or travel to the starting point of another one.

However, as a map or specific coordinates are not provided to the computer, in-bound course exploration may be necessary, so a task being listed in the scheduler is not enough for it to start running. The scheduler is sorted in a desired task completion order, but it is until the perception algorithms identify the starting position of a mission, that the vehicle decides: if the boat is relatively nearby and is not currently solving a task, the mission starts; otherwise, the vehicle navigates to said starting point after completing a running mission, jumps to a new task's state machine, and subsequently that task begins.

All tasks have their own state machines, which are updated through a method call on the same node in ROS 2 C++. Choosing the programming language was a huge factor, because all

missions are presented as inherited classes from a parent base class containing recurring general functions used on all state machines, and whenever a task jump is due, the shared pointer of the parent class points to another task's child class type. This pointer change happens for all tasks except for Task #5, which has its own variable just for itself to avoid messing up the interrupted task's state number.

C. Task 5 - Rescue Deliveries

Whenever a Task #5 obstacle is in a reachable position from the boat, regardless on whether a task is in process or not, a generated waypoint for station keeping is generated, in order to deliver water or balls depending on the type of vessel faced. If a task that is currently running is interrupted for Task #5, its state machine is not updated until Task #5 is completed. The generated waypoint on Task #5 is only for the vehicle to rotate towards the obstacle to deliver balls or water to, but if a translation is also needed to guarantee that the projectile reaches the target, a follow-up waypoint is generated after projectile deployment is confirmed, to go back to where the vehicle was before attempting Task #5, and continue with the stopped mission. This "stop and go" approach ensures that the scheduler order is not altered and the state machine of the interrupted task stays the same after addressing a Task #5 obstacle. The command for deploying a projectile is sent via the can bus all the way to the Mechanism PCB, which returns feedback indicating when deployment is confirmed.

Now that the Task #5 condition is addressed, the next tasks' approaches will be presented in order.

D. Task 1 - Navigation Channel

For Task #1, the mission starting point is 3 meters behind the first gate. A gate is a pose represented as a vector consisting of 3 elements: the 2D coordinates $[x,y]$ of the midpoint between two buoys, and an orientation which points along the normal to the segment from one buoy to another, corrected to the orientation closest to the current boat's heading (or else the heading is rotated 180°); this enables a path generation such that the boat will pass through said waypoint with the same orientation. In the state machine, the first waypoint is generated 1 meter ahead of the first gate, and when the boat has reached this waypoint, additional waypoints, 1 meter apart, are added until the next gate is found. Once reached a final waypoint 1 meter ahead is added.

E. Task 2 - Mapping Migration Patterns

Task #2 and Task #1 have the same starting point, this ensures the camera gets a view on all obstacles. The camera has a crucial role as it helps sort gates from reportable obstacles. It is important to state that no obstacle avoidance logic is tackled in any of the state machines, as the cascaded guidance-low level control scheme handles all obstacle avoidance, a significant upgrade from last year. At the start of the mission, a waypoint 1 meter ahead of the first gate is created. While the boat travels to this goal, the state machine keeps looking for more gates. When no other gate is found and the distance from the boat to the last registered goal is less than 0.5 m the task is completed.

F. Task 3 - Treacherous Waters

For Task #3, the boat is 4 meters in front of one of the two docking planes. The docking plane is the gate formed from the external banners. Based on experience from the arrangement on this task, the docking station is most likely to be placed near the edge of the course, so the finishing point of this task will be the face of the dock that is located the furthest from an edge (if it is not near an edge, the algorithm still returns a nearest face, this just works as an auxiliary feature to identify undiscovered starting task poses). The first state is to look, in the current docking plane, for a slot to travel to. If that slot is occupied, the appropriate waypoints are generated for the vessel to go to the other docking plane in the same relative position, 4 meters behind it. These waypoints are calculated given that both planes are parallel and the dimensions of the docking station are in the Team Handbook. To identify slot occupancy, clustering from the LiDAR is used (see Obstacle Dynamics Estimation), and if a cluster's euclidean center in the 2D plane is very close to what would have been a desired waypoint for the boat, that slot is considered to be occupied.

G. Task 4 - Race Against Pollution

Task #4 and Task #1 have the same starting point. The vessel enters the first gate and does station-keeping (discussed further in the document) with a certain navigation profile (see NMPC section) with a minor final rotation to ensure the LED panel is seen at all times. When the panel turns green, the navigation profile changes to the speed profile (see NMPC section), generating a waypoint in front of the second gate, and starts appending waypoints forward in 1 meter intervals until the blue buoy is detected. Once detected, the necessary waypoints to circle it are generated, as well as the waypoints to return to the starting position. All that is left to do is wait for the boat to cross the gate as fast as possible, to finish the task.

H. Task 6 - Return to Home

For Task #6, a waypoint is generated 1 meter behind the gate formed by the two black buoys. The main challenge is if a long distance must be traveled, and the docking station crosses the path. Because of the way our guidance and obstacle avoidance system works, small obstacles are avoidable, but bigger objects like the docking station are harder to avoid and may cause conflicts in the NMPC. If the docking station crosses the path to the starting position, additional waypoints are added before the guidance and NMPC system begin to operate.

II. DESIGN STRATEGY

In the following sections, the details for the technical decisions are explained for the software, mechanics, and electronics areas, showcasing how the newest iteration's changes contribute to better approach this year's autonomous challenge.

A. Software Architecture

This year, we retained the foundational structure of our ROS 2 workspace while upgrading our onboard computer from a Jetson TX2 to a Jetson Orin Nano. This transition proved highly beneficial, as the Jetson Orin Nano, paired with JetPack 6.1 (based on Ubuntu 22.04), natively supports ROS 2 Humble, aligning with the operating systems on our laptops. This eliminates the previous reliance on Docker containers for compatibility, streamlining our development and deployment processes.

B. Control Scheme

Inspired by VantTec's research spirit, we analyzed past controllers [Collado-Gonzalez et al. (2021b), Collado-Gonzalez et al. (2021c), Gonzalez-Garcia et al. (2022), Collado-Gonzalez et al. (2024)], their functionalities, and potential advancements. This led to developing a new control scheme combining Model Predictive Controller (MPC) features, like multi-objective optimization and model-based tracking-error minimization, with the robustness of Sliding Mode Control. The proposed approach integrates a Nonlinear Model Predictive Controller for path planning and guidance, cascaded with an Adaptive Integral Terminal Sliding Mode Controller, enabling the vehicle to navigate disturbed environments while avoiding obstacles detected through sensor fusion of a LiDAR and ZED stereo camera (Fig. 2).



Fig. 2. Diagram of the proposed multi-controller cascaded scheme.

C. Dynamic Model

The development of our controllers begins with deriving and parameterizing a Dynamic Model, which provides a detailed representation of how the vehicle responds to forces generated by the thrusters. This model serves multiple purposes: enabling accurate simulations, forming the foundation of the low-level state controller, and supporting predictions in the high-level guidance NMPC system. Following Fossen's (2011) formulation of a marine vessel's vectorial dynamic model:

$$M\dot{\nu} + C(\nu)\nu + D(\nu)\nu = \tau + \tau_{wind} + \tau_{wave} \quad (1)$$

, where

$$\eta = [x, y, \psi] \quad (2)$$

$$\nu = [u, v, r] \quad (3)$$

, where M refers to the system's inertial matrix, C is the Coriolis matrix, D is the dampening matrix, η stores the position and orientation of the vessel in 3 DOF from the inertial frame, and ν keeps the *surge*, *sway*, and *yaw* linear and angular velocities from the body frame (Fig. 15).

Through several calculations and experiments, it is possible to obtain their coefficients, which means that the behavior of the ASV can be modeled as a response from a τ input.

Based on 1, the decoupled equations of motion for *surge*, *sway*, and *yaw*, and x , y , and ψ describe the complete nonlinear dynamic model:

$$\dot{u} = \frac{1}{m - X_{\dot{u}}}[(m - Y_{\dot{v}})vr + X_{u|u}|u| + X_u u + \tau_x] \quad (4)$$

$$\dot{v} = \frac{1}{m - Y_{\dot{v}}}[(-m + X_{\dot{u}})ur + Y_{v|v}|v| + Y_v v] \quad (5)$$

$$\dot{r} = \frac{1}{I_z - N_{\dot{r}}}[-X_{\dot{u}} + Y_{\dot{v}})uv + N_{r|r}|r| + N_r r + \tau_r] \quad (6)$$

$$\dot{x} = u \cos(\psi) - v \sin(\psi) \quad (7)$$

$$\dot{y} = u \sin(\psi) + v \cos(\psi) \quad (8)$$

$$\dot{\psi} = r \quad (9)$$

D. Adaptive Integral Terminal Sliding Mode Controller

On the other hand, to control the low-level states of *surge* and ψ , a model-based Sliding Mode Controller is the proposed strategy because of its robustness against disturbance, and a relatively fast and assured convergence.

Given the extension of the procedure, it is explained in Appendix D.

E. Nonlinear Model Predictive Controller

The final component of the control scheme is the NMPC, which integrates path planning, guidance, and obstacle avoidance into a single algorithm. This approach is particularly valuable for this project due to its ability to perform real-time multi-objective optimization, enforce constraints, and adapt flexibly to varying control objectives.

For the NMPC's model states, equations 4-9 are used to predict the vessel's dynamics over a given horizon. Additionally, the model incorporates the dynamics for n buoys. Because their velocity directly affects their position, it is proposed that considering this factor in the NMPC's model may help the ASV avoid collisions better. By knowing the x and y velocity components of each obstacle, their dynamics can be integrated into the NMPC model:

$$\dot{obs}_{x_i} = obs_{d_{x_i}} \quad (10)$$

$$\dot{obs}_{y_i} = obs_{d_{y_i}} \quad (11)$$

To define a control objective for the controller to optimize, the following performance indicators are defined:

$$y_e = -[x - x_k] \sin(\alpha_k) + [y - y_k] \cos(\alpha_k) \quad (12)$$

$$x_e = [x - x_k] \cos(\alpha_k) + [y - y_k] \sin(\alpha_k) \quad (13)$$

$$\psi_e = \psi - \alpha_k \quad (14)$$

where y_e y x_e are the cross-track and along-track error, respectively, and ψ_e is the heading error. Furthermore, for avoidance, an indicator (eq. 15) was designed, with a rational function-like behavior, which elevated to a power can be tuned to acquire more weight when approaching an obstacle, while becoming negligible otherwise.

$$cost = \frac{1}{distance_i^k} \quad (15)$$

Therefore, the following nonlinear problem for the optimization program to solve is designed:

$$\begin{aligned} \min \sum_{i=0}^{N-1} & \|y_{e,i}\|_{Q_{y_e}}^2 + \|\psi_{e,i}\|_{Q_{\psi}}^2 + \|x_{e,i}\|_{Q_{x_e}}^2 + \|u_i\|_{Q_u}^2 \\ & + \|r_i\|_{Q_r}^2 + \sum_{j=0}^{av_n} \frac{Q_{ds}}{d_{k,j}^{3/2}} + \|y_{e,N}\|_{Q_{N,y_e}}^2 + \|\psi_{e,N}\|_{Q_{N,\psi}}^2 \\ & + \|x_{e,N}\|_{Q_{N,x_e}}^2 + \|u_N\|_{Q_{N,u}}^2 + \|r_N\|_{Q_{N,r}}^2 + \sum_{j=0}^{av_n} \frac{Q_{N,ds}}{d_{k,j}^{3/2}} \end{aligned} \quad (16)$$

The nonlinear problem's objective is to minimize the result of the sum, where the Q s refer to the accumulative weights and the Q_N s refer to the terminal weights, ensuring that not only the whole trajectory is optimized, but also, that the vehicle does reach its goal. It is proposed that each of these Q s are dynamic parameters that affect the NMPC's avoidance profile depending on the scenario the vehicle is in. This is important, because the testing scenario for the control scheme is a speed challenge, where the vehicle must go as fast as it can while avoiding all collisions, and the algorithm is therefore able to choose between going slow and steady if there are no obstacles nearby, or fast and less careful otherwise. $\sum_{j=0}^{av_n} Q_{ds} d_j^{-3/2}$ is the sum of the distances from the k nearest obstacles to each of 5 points making up a polygon (fig. 16) surrounding the vehicle, to ensure that the whole vessel avoids collisions, not just one region.

Finally, the system's restrictions are:

$$\begin{aligned} -30 & \leq T_{port} \leq 36.5 \\ -30 & \leq T_{stbd} \leq 36.5 \end{aligned} \quad (17)$$

, which are the physical limitations on the T200 electric motors from Blue Robotics, used as the control input on the NMPC's model, which output is not sent directly to the thrusters' ESCs, as the AITSMC is the one in charge of providing that signal, but this way, realistic *surge* and *yaw* dynamics are considered in the model.

F. Obstacle Dynamics Estimation

The implemented pipeline is adapted from traffic segmentation techniques to enable obstacle detection for an unmanned surface vehicle (USV) in open waters:

- 1) **Data Cleaning and Filtering:** The raw LiDAR data is preprocessed to remove noise and irrelevant points.
- 2) **Removal of Lowest Points:** A RANSAC algorithm is applied to eliminate low-lying points, which could correspond to water surfaces.
- 3) **Clustering:** Clusters are extracted using Euclidean Cluster Extraction algorithms, with a Kd-Tree data structure used to manage the cluster organization.

Initially, the raw point cloud is processed using a Pass-through Filter to remove points outside a predefined range. Next, a Voxel Grid filter reduces the samples of the point cloud in order to reduce data density while retaining essential spatial information. Surface normals are calculated, and the RANSAC algorithm is employed to exclude residual points corresponding to the water surface if the Pass-through Filter fails to remove them. Notably, testing revealed that the LiDAR rarely detected the water surface. Clusters are then identified using Euclidean Clustering within a specified range. Once clustering is complete, each object is approximated using two models: a bounding box and a sphere. The sphere is centered on the centroid of the cluster, with its radius calculated as the average distance from the centroid to the points of the cluster.

With the clustered obstacles, we can globally register and label each obstacle based on attributes such as color, size, or shape, through a transformation from the boat's local frame into the world frame. This approach is particularly useful for identifying the starting points of specific tasks. Furthermore, since the LiDAR has a minimum detection range of approximately 1 meter, obstacles that are no longer visible in the scan can still be accounted for. By maintaining a record of their locations, the boat remains aware of their presence, ensuring that the NMPC considers these obstacles during navigation to maintain safe operation.

In addition to the LiDAR, the ZED Stereo 2 camera provides a pixel-to-position mapping capability, enabling a similar registration process. More importantly, this system supports object tracking using the clusters' positions, which allows for the calculation of position changes over time. This, in turn, enables the estimation of the dynamics of each cluster. Feeding these dynamics into the NMPC is critical, as static obstacle avoidance tests demonstrated no delays in the controller's response; however, dynamic obstacle avoidance tests revealed significant performance issues when obstacle dynamics were not considered, leading to their inclusion in the solution.

This capability is especially beneficial in scenarios where buoys may drift due to strong waves, or objects become detached from their anchors, as it ensures dynamic adjustments for safer navigation.

G. Waypoint Handling

Now that the control scheme is explained, what we have is: 1) a mission handler node that receives data from perception and the vehicle's pose, and outputs desired waypoints for the boat to follow, and 2) a control scheme that receives continuous 10Hz references for the boat to reach alongside obstacles' dynamics information, and outputs a desired PWM

for each thruster. The bridge between these two systems, is the waypoint handler node, which serves to generate a smooth and feasible trajectory for the boat. This node is responsible for interpolating the sequence of waypoints provided by the mission handler into a continuous path that the control system can accurately follow. Additionally, it incorporates dynamic constraints of the vehicle, such as its maximum speed and turning radius, ensuring that the planned trajectory remains executable. The waypoint handler also monitors the progress of the vehicle, dynamically updating the active waypoint to account for deviations or unexpected obstacles encountered during the mission.

Given that the waypoint handler generates the desired trajectory for the boat, when it stops generating a path, generally because the vehicle reached a waypoint, the boat is in a station-keeping state, because the waypoint handler is telling the NMPC that it should keep the same heading and a linear velocity of zero.

H. Electronics Design Strategy

In last year's competition, the team utilized phenolic circuit boards for the subsystem dedicated to the water delivery and object task but encountered problems with connections that frequently disconnect. To address this, we designed, manufactured, and soldered object and water-delivery mechanism PCBs to enhance reliability by relying on Molex connectors to substitute jumper connections.

To improve teleoperation capabilities, radio frequency modules with a wider communication range were acquired and incorporated into the radio communication subsystem. The electronic organization of the new vehicle prioritized easy accessibility by storing all components in a waterproof electronic box (3).

I. Object and Water Delivery Mechanism PCB

The Object and Water Delivery Mechanism PCB was designed to control key components of its dedicated system, including a water pump, a waterproof motor, and a NEMA 23 motor, while also supporting additional external modules and actuators that require +3.3V or +5V. It features an STM32 microcontroller that communicates with other USV system nodes, such as the main STM32 PCB, via a CANBus transceiver, and includes connectors for I2C and UART communication. This PCB was based on the main STM32 PCB of the vehicle.

The PCB includes two H-bridges for controlling the water pump and waterproof motor, along with a through-hole interface for a TMC2208 driver to operate the NEMA 23 motor, ensuring actuation and system integration (See design in Appendix C).

J. Mechanical Design Strategy

The boat's design is inspired by a Catamaran structure, utilizing laser-cut balsa wood for easy assembly with rib connections secured by nylon straps. Foam fills the empty spaces to provide emergency buoyancy. The structure is reinforced with carbon fiber coated in multiple epoxy layers,

with sanding between applications and a varnished layer for UV protection. Profiles connect the pontoons and house a waterproof electronic box. Additional features include thruster mounts for easy propeller installation and removal, stabilizers for the stereo camera and LiDAR sensors, and a custom PCB for controlling water pumps, motors, and external actuators.

Using tools such as Solidworks and ANSYS Simulation, the mechanics' department focused its efforts on designing a modular, easy-to-transport, stable, and hydrodynamic boat while keeping a robust structure. Modularity gives the team the ability to rapidly adapt the boat, like adding, modifying, or repairing components, due to the constant testing and development the prototype undergoes. Also, as it is necessary to transport the ASV, the design is more compact and can be easily disassembled. Finally, a more stable and hydrodynamic boat means more maneuverability for the boat to rapidly complete tasks with effective power usage and achieve buoyancy with around a 30% draft line.

K. Hull Design

The hull design for this year's ASV was inspired by the "Tesla Catamaran" design by Tech Ingredients. Following his recommendation, a NACA-0008 profile was generated to use as a base design in our main CAD tool: Solidworks. The original idea was to modify the profile applying a reverse bow profile due that it breaks waves with ease. The buoyancy of each of these 4 iterations was calculated considering that the buoyant force is $F=Vg$ and the weight of the cargo is $W=mg$. Since the boat needs to be positively buoyant, then the displaced volume of water needs to be greater than the cargo mass divided by the fluid's density (water) V_m . Using Solidworks physical properties calculator, this minimum volume can be found to denote the draft line. As studied in the Applied Naval Architecture book, by Robert B. Zubaly, it is recommended that the draft line is around 35% of the pontoon's total height. After finding the draft line for all the iterations, CFD simulations with same conditions were performed to confirm which design will have the best performance (Appendix E), and the NACA design presented the best results. The average drag force was reduced 68% compared to the past design, with a value of 0.393 N. This happened because the design is smaller, with a length of 1 meter and a height of 25 cm, to reduce fabrication costs, facilitate transportation, and increase maneuverability. Conservation of velocity was at 99% and the simulations also show how a low pressure zone behind the hull is created, which indicates hydrodynamic behavior. Other characteristics to point out about the design is that its center of flotation is 10 cm from the bottom, and 47.6 cm from the front, meaning it is in the low-front. It is expected that the boat is stable laterally and longitudinally since the center of flotation will be allocated near the symmetrical center. Finally, the manufacturing of these hulls will consist of laser cutting balsa wood with lattice hinge marks to facilitate forming, using a stitch n' glue technic to complete the hull and finally covering the surface with carbon fiber and epoxy resin.

L. Modular Structural System

The main structure of the ASV is built with M20 aluminium profiles by EINSMODULAR, along with brackets and T screws. 3 horizontal profiles join the two pontoons, while 2 longitudinal profiles reinforce the structure to avoid rotation of the pontoons. The main advantage of using M profiles is that the structure can be modified as necessary to arrange components such as the LiDAR sensor and the ZED camera. The selection of this profiles was based on the deflection that the profile would withstand. Considering the thrusters have a 60 N force, with a second moment of area of 0.8 cm⁴, a 70 GPa elasticity modulus (provided by the manufacturer), and this profiles would be restricted to a length of 644 mm. Using the formula:

$$f = \frac{FL^3}{3EI10^4} \quad (18)$$

for a flying beam, the deflection would be evenly distributed in 3 profiles with a value of 2.12 mm.

M. Ball and Water Delivery Mechanism

This mechanism features a ball shooter driven by a DC motor with a belt system. This design ensures precise and reliable delivery of objects during tasks. Its design allows for easy maintenance and upgrades, ensuring robust performance in various competition scenarios. This system is crucial for tasks requiring accurate object delivery, although not that much balls will be needed. (See design in Appendix F)

N. Propulsion System

The propulsion system consists of four T200 thrusters from BlueRobotics, two per pontoon. These are not integrated on the hull, but rather installed using a mount with a main and secondary part. This mount design was developed so that it is simpler to remove, maintain and replace the thrusters or the mount in case they break. The mount also works as a safety mechanism, so damage does not propagate to the hull. (See design in Appendix F).

The most significant improvement to the thruster mounts is the addition of ribs in the connection zone, doubling the part's stiffness to better withstand force and distribute stress more effectively. The part is fabricated using FDM printing using Bambu Lab's polycarbonate filament. This modification ensures stress is concentrated on a small point rather than on the corners, enhancing durability and reliability.

III. TESTING STRATEGY

The testing strategy was designed to evaluate the vessel's capabilities and ensure its aptness for competition. Initial testing included validating thruster control via CAN and trajectory-following algorithms using simulations and preliminary dry runs. Electronic mechanisms were tested individually and then integrated into the system under the same power supply and isolation conditions. Software and perception algorithms were tested in a simulation environment to assess path-following performance. Each competition task was tested in real-world conditions. Finally, a full autonomous competition-like course

was conducted, prioritizing tasks with higher success rates and awards.

A. Simulator Testing

Simulator testing in Gazebo was crucial for evaluating the vehicle's movement and performance in various challenges. This approach allowed rapid validation of decision-making algorithms and logic without the delays and randomness of in-water testing. It provided a controlled environment to improve the performance of the vehicle before doing physical tests.

B. Dry Testing

Dry testing focused on validating hardware and algorithms. Brief propeller functionality tests and perception systems, including stereo cameras and LiDAR sensors, were tested in laboratory settings by placing them in front of buoys and other items. This ensured that we confirmed the reliability of the algorithms and the correct integration of hardware components.

C. In-Water Testing

In-water testing was made at external facilities, such as the Borregos swimming pool from our institution, the aquatic center in Nuevo León from the High Performance Center (CARE) and even the town of Santiago's Presa La Boca. These tests validated the functionality of modules such as the stereo camera, the LiDAR sensor, the IMU, GNSS and RTK antennas, task-specific code and improved perception algorithms in real-world conditions. Access to them enabled the team to improve performance, bridging the gap between simulation and competition preparedness.

ACKNOWLEDGMENTS

VantTec extends its gratitude to our corporate sponsors for their support in funding and resource provision, including Techmake, RoboNation, Velodyne LiDAR, MECA LABS, ALL WAYS SUNNY, and EPOXMEX. We are also grateful to Tecnológico de Monterrey, the School of Engineering and Sciences, Monterrey's administration, the National SES, the Department of Mechatronics for their funding and access to equipment for the manufacturing of the redesigned pontoons and the overall vehicle design, and the Centro de Alto Rendimiento (CARE). Their support included access to the Wellness Center Borregos swimming pool for indoor in-water testing and three competitive swimming pools for outdoor testing.

We particularly thank our advisors, Dr. Herman Castañeda and Dr. Alberto Muñoz, for their expertise and guidance in developing the predictive controller model for vehicle control systems and the immeasurable amount of faith and support they have given to our group. Lastly, we express our appreciation to our alumni, whose contributions, interest and passion were key in making this project successful.

REFERENCES

- [1] Collado-Gonzalez, I., Gonzalez-Garcia, A., Sotelo, C., Sotelo, D., & Castañeda, H. (2021b). A Real-Time NMPC Guidance Law and Robust Control for an Autonomous Surface Vehicle. IFAC-PapersOnLine, 54(16), 252-257. <https://doi.org/10.1016/j.ifacol.2021.10.101>
- [2] Collado-Gonzalez, I., Gonzalez-Garcia, A., Sotelo, C., Sotelo, D., & Castañeda, H. (2021c). A Real-Time NMPC Guidance Law and Robust Control for an Autonomous Surface Vehicle. IFAC-PapersOnLine, 54(16), 252-257. <https://doi.org/10.1016/j.ifacol.2021.10.101>
- [3] Gonzalez-Garcia, A., Collado-Gonzalez, I., Cuan-Urquiza, R., Sotelo, C., Sotelo, D., & Castañeda, H. (2022). Path-following and LiDAR-based obstacle avoidance via NMPC for an autonomous surface vehicle. Ocean Engineering, 266, 112900. <https://doi.org/10.1016/j.oceaneng.2022.112900>
- [4] Collado-Gonzalez, I., Gonzalez-Garcia, A., Cuan-Urquiza, R., Sotelo, C., Sotelo, D., & Castañeda, H. (2024). Adaptive sliding mode control with nonlinear MPC-based obstacle avoidance using LiDAR for an autonomous surface vehicle under disturbances. Ocean Engineering, 311, 118998. <https://doi.org/10.1016/j.oceaneng.2024.118998>
- [5] Fossen, T. I. (2011). Handbook of Marine Craft Hydrodynamics and Motion Control. <https://doi.org/10.1002/9781119994138>
- [6] Tech Ingredients. (2019, 11 octubre). The Tesla Catamaran! [Vídeo]. YouTube. <https://www.youtube.com/watch?v=6BMsksLiYA>
- [7] Zubaly, R. B. (2009). Applied Naval Architecture. https://openlibrary.org/books/OL811108M/Applied_naval_architecture

APPENDIX A: TEST PLAN AND RESULTS

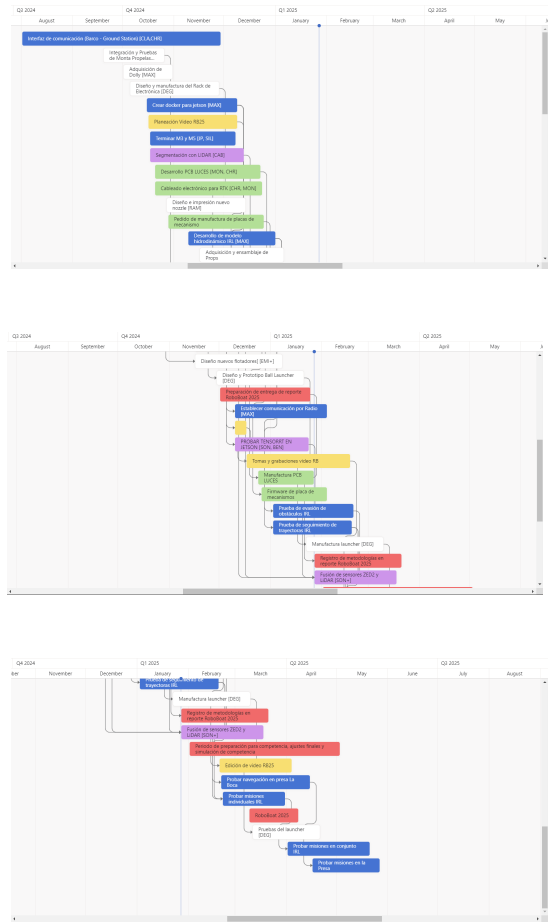
Scope

The test plan objectives focused on ensuring the correct functionality of VantTec's electronic modules and validating basic algorithmic solutions for this year's competition tasks. Tests included verifying performance for obstacle detection and inertial measurement data accuracy using LiDAR and IMU sensors. Reliable navigation, trajectory following and obstacle avoidance were rigorously tested in controlled environments, such as the Borregos Wellness Center and Centro de Alto Rendimiento swimming pools, as well as in natural water bodies like the Presa la Boca reservoir.

Schedule

In August 2024, the VantTec RoboBoat team developed a Gantt chart to organize the workflow and align efforts toward achieving the goal of winning RoboBoat 2025. Three general team sprint meetings were held with the group's other autonomous vehicle projects to review progress as well as several subteam and chief area meetings across the team's four core areas: Mechanics, electronics and embedded systems, software and perception. Tasks for each subteam were assigned specific deadlines spanning from August 3, 2024, to February 9, 2025, to ensure the vehicle's full functionality. Testing sessions were

scheduled throughout this period, including multiple visits to the Borregos Wellness Center swimming pools for afternoon Sunday access and three December sessions at the Centro de Alto Rendimiento swimming pools, with access from 10:00 AM to 3:00 PM.



Resource and Tools

For simulation testing, ROS2, RViz, and Gazebo were essential tools, enabling the visualization and execution of the vehicle's navigation, trajectory following, obstacle avoidance, and task execution logic in a controlled environment free from external perturbations. These simulations were critical for refining the system before physical testing.

A range of hardware components support both dry and in-water testing. These included a Jetson computer, an STM32 PCB, two power distribution PCBs, an object and water delivery mechanism PCB, two 14.8V BlueRobotics LiPO batteries, four T200 thrusters with basic BlueRobotics ESCs, and two LM2596 +5V buck converters. Sensors and peripherals included a Velodyne VLP16 LiDAR, SBG Systems Ellipse2-D IMU with GNSS antennas, a ZED2 stereo camera, an X8R receiver for mode selection, an XBee antenna, and a HolyBro Telemetry Radio.

Dry testing validated thruster control and direction, ensured reliable object detection and classification based on shape and color. In-water testing confirmed the sealing of the pontoons,

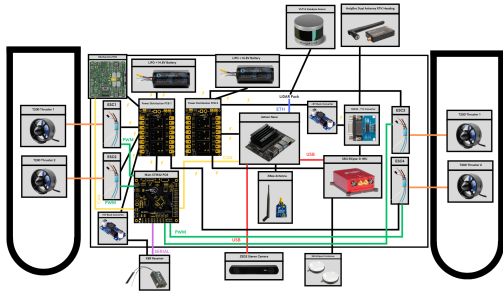


Fig. 3. Connection diagram of electronic components of the USV.

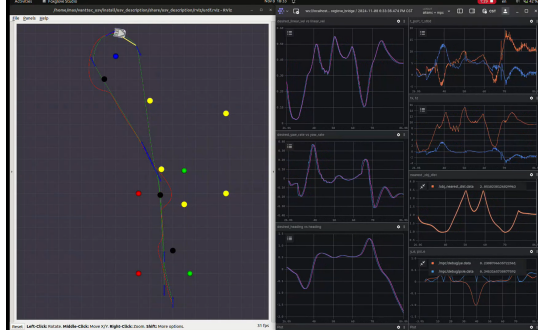


Fig. 4. Static and dynamic obstacle avoidance with Non-Linear Model Predictive Controller.

the vehicle's resistance to water perturbations, thruster functionality, and the performance of the LiDAR, IMU, GNSS, Xbee and RTK antennas, X8R receiver, and ZED2 stereo camera.

Environment

Simulation tests utilized an existing 3D competition field model of Nathan Benderson Park, the Open Source Robotics Foundation, combined with the 3D CAD model of the V-TEC-S-IV. For dry testing, the unmanned surface vehicle mounted on its dolly cart facilitated evaluations of hardware and algorithm functionality, especially computer vision.

In-water testing was conducted at three locations: The Borregos Wellness Center's semi-Olympic swimming pool with a depth of two meters and a temperature range of 26 to 29°C, provided a controlled environment for initial tests. The Centro Acuático at the Centro de Alto Rendimiento from Nuevo León offered Olympic and semi-Olympic pools in an open-air setting, allowing for the testing of GNSS functionality. Lastly, the Presa La Boca reservoir in Santiago, Nuevo León, offered a natural environment with conditions similar to Nathan Benderson Park's lake, featuring more significant water perturbations to test the vehicle's performance.

Risk Management

The VantTec RoboBoat team ensured effective risk management through coordinated efforts led by the president, project engineering leader and project management leaders. They managed communication with institutions and communities



Fig. 5. In-water testing of V-TEC-S-IV in the Centro de Alto Rendimiento's semi-Olympic swimming pool.

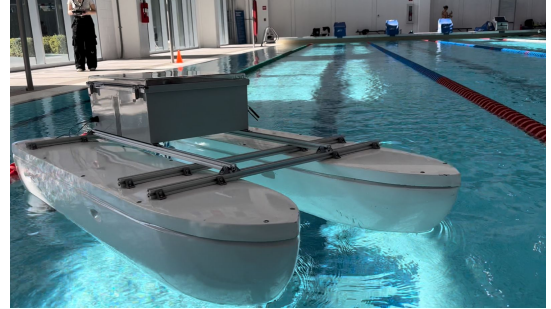


Fig. 6. In-water testing of V-TEC-S-IV in Wellness Center semi-Olympic swimming pool.

that provided the testing environments, prepared and submitted all paperwork, and secured approvals.

Safety measures during testing included individual pontoon sealing checks and continuous vehicle inspections while in swimming pools. A team member remained in the water during these tests, except at Presa La Boca, where water exposure was limited to knee level. To prevent accidents, two ropes were attached to the boat, allowing members to maintain a secure grip and respond in the event of submergence or water leakage. These precautions ensured the safety of both team members and the vehicle.

Results

The VantTec RoboBoat team gathered critical insights during testing, such as the effectiveness of pontoon sealing,

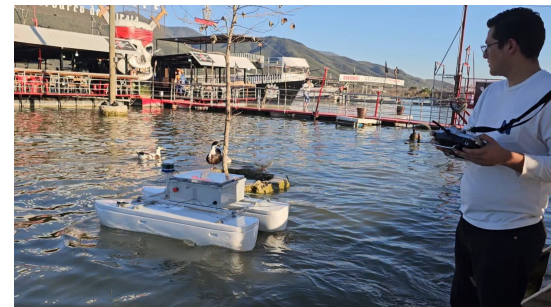


Fig. 7. V-TEC-S-IV in-water testing of modules and algorithms in Presa La Boca, Santiago, N.L., Mexico.

prevention of water leakage, and optimal weight distribution of components and modules for improved buoyancy and hydrodynamics. ROS2 Bags were recorded during each session to collect data that contributed to refining the vehicle's Non-Linear Model Predictive Controller and calibrating sensors such as the IMU and GNSS antennas. These recordings allowed team members unable to attend specific testing sessions to analyze the data and incorporate the learnings into improvements, ensuring progress.

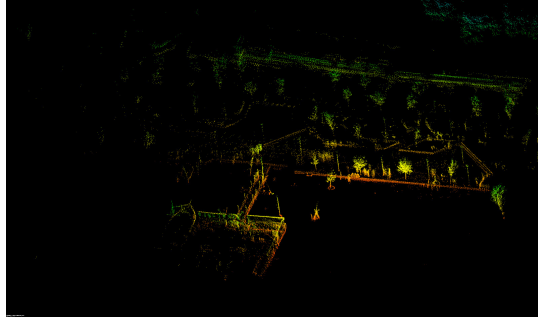


Fig. 8. First visualization of LIO-SAM environmental map from dry-testing in Presa la Boca reservoir.

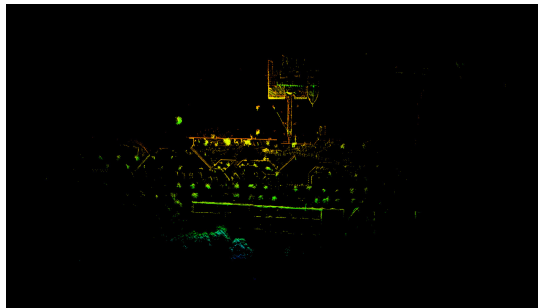


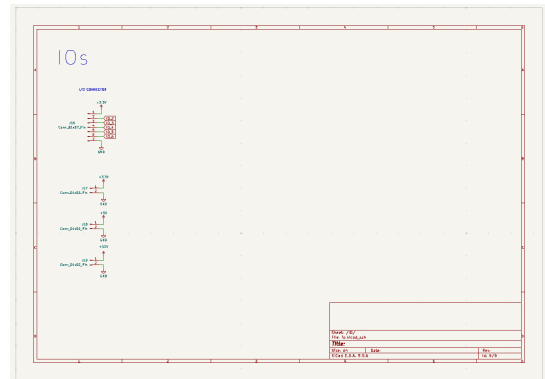
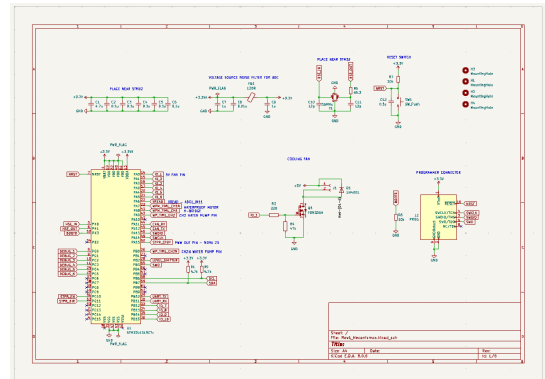
Fig. 9. Second visualization of LIO-SAM environmental map from dry-testing in Presa la Boca reservoir.

APPENDIX B: COMPONENTS LIST

	Vendor	Model / Type	Specs	Custom / Purchased	Cost	Year of Purchase
ASV Hull Form / Platform	1) Tecnológico de Monterrey School of Engineering and Sciences 2) VanITec	1) Pontoon 2) Catamaran	1) Donation from the School of Engineering and Sciences 2) Manufactured by participating team.	Custom	1) Donated from the school, 2) Sponsored Resin & Carbon Fiber, \$50 Balsawood	2025
Waterproof Connectors	BlueRobotics	WetLink Penetrator	https://bluerobotics.com/store/cables-ic-connectors/penetrators/wlp-vol/	Purchased	\$16	2024
Propulsion	BlueRobotics	T200 Thruster	https://bluerobotics.com/store/thrusters/t200-thrusters/t200-thrusters-2-pc/	Purchased (4)	\$200	2024
Power System	BlueRobotics, HobbyKing	Lithium-Ion Battery, ZIPPY Compact 800mAh 3S1P 30C	https://docs.bluerobotics.com/batteries/tips-hobbyking.com/en-us/zippy-y-compact-800mah-3s1p-30c-lipo-pack-with-x150-lithiflug-bv019k2T03JnBh2ZU9MSZxvWVxvzGv0b9zZWfVY2hYt2hu5GVudD0=	Purchased (2) Purchased (2)	\$350, \$70	2018, 2022

Motor Controls	BlueRobotics	Basic ESC R2	https://bluerobotics.com/store/thrusters/speed-controllers/basic-esc-30-r2/	Purchased	\$38	2017
CPU	NVIDIA	Jetson TX2	https://developer.nvidia.com/embedded/buy/jetson-tx2	Purchased	Sponsored	2018
Teleoperation	FrSky	Taranis X9D, XBR	https://www.frsky.com/product/taranis-x9d-plus-2/ https://www.frsky.com/product/x8r/	Purchased	Sponsored	2017
Compass						
Inertial Measurement Unit (IMU)	SBG Systems	SBG Ellipse2-D	https://www.sbg-systems.com/products/ellipse-series	Purchased	Sponsored	2017
Doppler Velocity Logger (DVL)						
Camera(s)	Stereolabs	ZED Camera	https://www.stereolabs.com/zed/	Purchased	\$499	2017
Hydrophones						
Algorithms	VanITec Development					
Vision	Point Cloud Library, OpenCV, YOLOv8					
Localization and Mapping	VanITec Development					
Autonomy	VanITec Development					
Open Source Software	ROS2, Python, C++, Matlab, Pytorch					

APPENDIX C: WATER AND OBJECT DELIVERY MECHANISM PCB



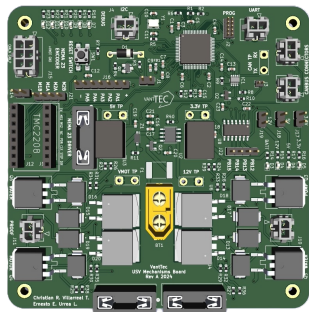
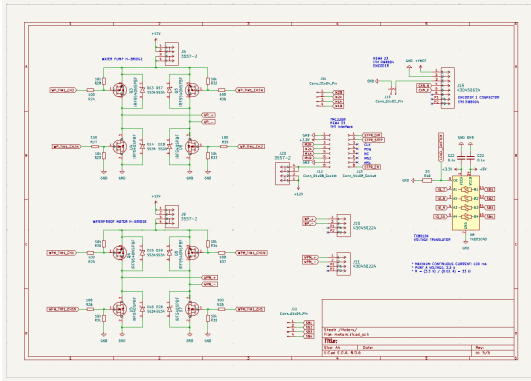
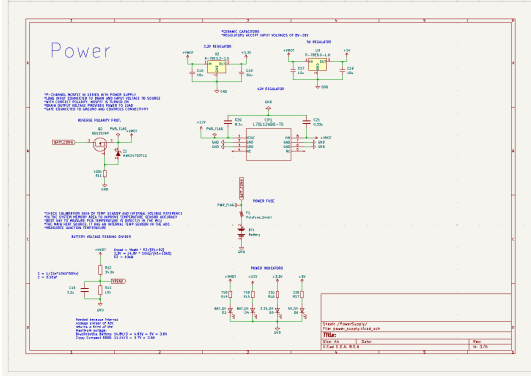
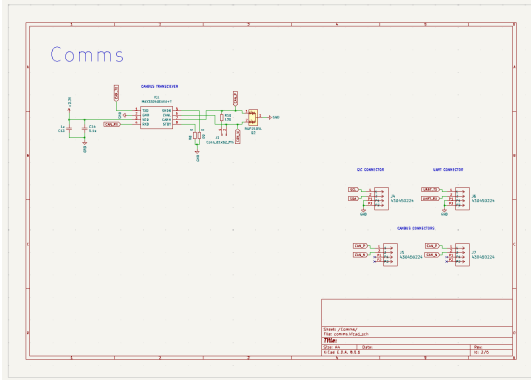


Fig. 10. 3D visualization of Object and Water Delivery Mechanism PCB.

APPENDIX D: ADAPTIVE INTEGRAL TERMINAL SLIDING MODE CONTROLLER PROCEDURE

Based on 4 and 6, each definition can be written as:

$$\dot{\zeta}_u = f(\zeta_u) + g(\zeta_u)U_u \quad (19)$$

$$\dot{\zeta}_\psi = f(\zeta_\psi) + g(\zeta_\psi)U_\psi \quad (20)$$

, where

$$f(\zeta_u) = \frac{1}{m - X_{\dot{u}}}[(m - Y_{\dot{v}})vr + X_u|u|u + X_u u] \quad (21)$$

$$g(\zeta_u) = \frac{1}{m - X_{\dot{u}}} \quad (22)$$

$$U_u = \tau_x \quad (23)$$

$$f(\zeta_\psi) = \frac{1}{I_z - N_{\dot{r}}}[(-X_{\dot{u}} + Y_{\dot{v}})uv + N_{r|r}|r|r + N_r r] \quad (24)$$

$$g(\zeta_\psi) = \frac{1}{I_z - N_{\dot{r}}} \quad (25)$$

$$U_\psi = \tau_r \quad (26)$$

with τ_x and τ_r as the forces [N] generated by the differential distribution of the motors representing the linear force in *surge* and the angular force in *yaw*. Furthermore, a sliding mode control strategy considers a sliding surface variable whose definition varies depending on the order of the controller (first and second order, respectively, for *surge* and ψ). Therefore, the following sliding surfaces are defined:

$$s_u = e_u + \alpha_u e_{I,u} \quad (27)$$

$$\dot{e}_{I,u} = \text{sign}(e_u)|e_u|^{q_u/p_u} \quad (28)$$

$$s_\psi = \dot{e}_\psi + \beta_\psi e_\psi + \alpha_\psi e_{I,\psi} \quad (29)$$

$$\dot{e}_{I,\psi} = \text{sign}(e_\psi)|e_\psi|^{q_\psi/p_\psi} \quad (30)$$

where

$$e_u = u_d - u \quad (31)$$

$$e_\psi = \psi_d - \psi \quad (32)$$

, α_u , β_u , q_u , p_u , α_ψ , β_ψ , q_ψ , and p_ψ are tunable parameters describing the sliding surfaces' behavior, and $e_\psi \in (-\pi, \pi]$. Also, their derivatives are:

$$\begin{aligned} \dot{s}_u &= \dot{e}_u + \alpha_u \dot{e}_{I,u} \\ &= \dot{u}_d - \dot{u} + \alpha_u \dot{e}_{I,u} \\ &= \dot{u}_d - (f(\zeta_u) + g(\zeta_u)U_u) + \alpha_u \dot{e}_{I,u} \end{aligned} \quad (33)$$

$$\begin{aligned} \dot{s}_\psi &= \ddot{e}_\psi + \beta_\psi \dot{e}_\psi + \alpha_\psi \dot{e}_{I,\psi} \\ &= \dot{r}_d - \dot{r} + \beta_\psi \dot{e}_\psi + \alpha_\psi \dot{e}_{I,\psi} \\ &= \dot{r}_d - (f(\zeta_\psi) + g(\zeta_\psi)U_\psi + \beta_\psi \dot{e}_\psi + \alpha_\psi \dot{e}_{I,\psi}) \end{aligned} \quad (34)$$

, when the sliding surface is kept at zero, the controller ensures finite-time convergence, guaranteeing that the desired reference will be achieved. With this representation, it is possible to substitute the forces (U with their equivalent in τ) and solve for them to determine the desired thrust:

$$\tau_u = \frac{1}{g(\zeta_u)} [-f(\zeta_u) + \dot{u}_d + \alpha_u \dot{e}_{I,u} - u_{\alpha,u}] \quad (35)$$

$$\tau_r = \frac{1}{g(\zeta_r)} [-f(\zeta_r) + \dot{r}_d + \alpha_r \dot{e}_{I,r} - u_{\alpha,r}] \quad (36)$$

, where u_a is the adaptive auxiliary control signal proposed with the AITSMC strategy, which is defined for *surge* and *heading* as:

$$u_{a,u} = -K_{1,u} |s_u|^{(1/2)} \text{sign}(s_u) - \varepsilon_u K_{1,u} |s_u| \quad (37)$$

$$\dot{K}_{1,u} = \alpha_u^{(1/2)} |s_u|^{(1/2)} - \beta_u^{(1/2)} |K_{1,u}|^2 \quad (38)$$

$$u_{a,\psi} = -K_{1,\psi} |s_\psi|^{(1/2)} \text{sign}(s_\psi) - \varepsilon_\psi K_{1,\psi} |s_\psi| \quad (39)$$

$$\dot{K}_{1,\psi} = \alpha_\psi^{(1/2)} |s_\psi|^{(1/2)} - \beta_\psi^{(1/2)} |K_{1,\psi}|^2 \quad (40)$$

$$0 < \varepsilon_u < 1, \quad 0 < \varepsilon_\psi < 1$$

$$0 < \alpha_u, \quad 0 < \beta_u$$

$$0 < \alpha_\psi, \quad 0 < \beta_\psi$$

APPENDIX E: MECHANICAL DESIGN SIMULATION FOR HULL PERFORMANCE COMPARISON

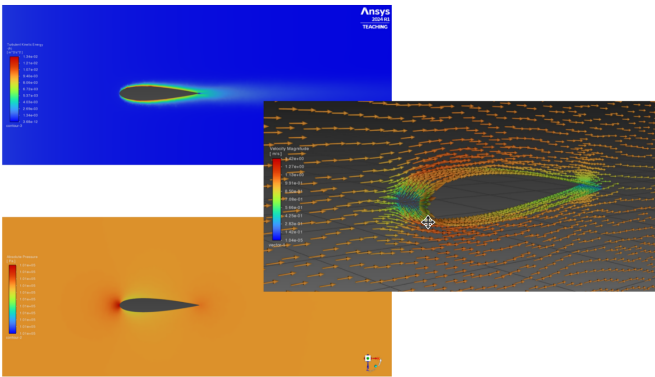


Fig. 11. Kinetic Turbulence Energy (top left), Absolute Pressure (bottom left), and Velocity (middle right).

The Naca 008 airfoil is usually used in aeronautics, but we decided to use it because of its low current flow and low hydrodynamics.

The hydrodynamic efficiency is due to the low drag coefficient. The symmetry allows a balance of hydrodynamic forces. A simulation in Ansys demonstrated a drag coefficient of 0.23, proving the malleability of the airfoil.

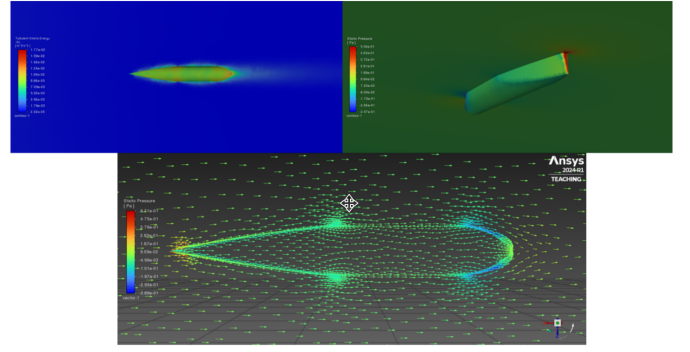


Fig. 12. Kinetic Turbulence Energy (top left), Static Pressure (top right and down).

In this new design prevents flow separation. This was accomplished by modifying the original NACA profile, optimizing it to reduce turbulence. A drag coefficient of 0.17 has achieved with this new design. Giving an increase of

$$26\% = \frac{0.23-0.17}{0.23} * 100$$

in performance for the drag coefficient.

The reduced wake turbulence indicates lower energy losses, resulting in greater energy efficiency. The hull design promotes laminar flow, reducing impact and energy source consumption.

At the bow of the new ship design, static pressure is lower compared to traditional designs but remains sufficient to ensure stability and vertical thrust. Along the hull, pressure is evenly distributed with a smooth transition. The low pressure at the bow implies less frontal resistance, which reduces the pressure drag coefficient. The uniform pressure distribution prevents structural stress points on the hull, prolonging material lifespan.

The reduced drag ensures that the vessel requires minimal power to reach and maintain high speeds in the water. The near absence of kinetic turbulence in the wake significantly decreases energy losses and improves downstream flow behavior. Finally, the design's low bow and uniform pressure distribution around the hull to reduce resistance in the forward motion.

APPENDIX F: MECHANICAL DESIGNS

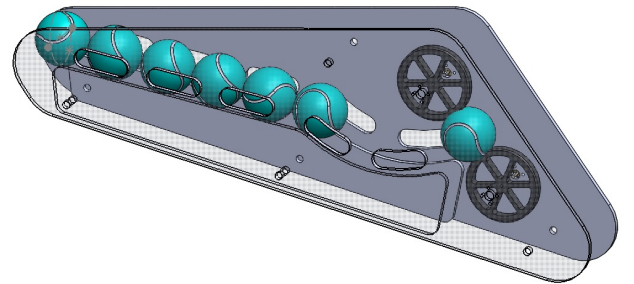


Fig. 13. Mechanism CAD draft, not yet shrunk for fewer ball holdback.

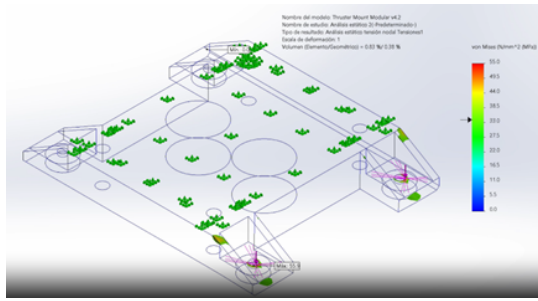


Fig. 14. Final Iteration of the Thruster Adapters for Propulsion.

APPENDIX G: SUPPORT MATERIAL

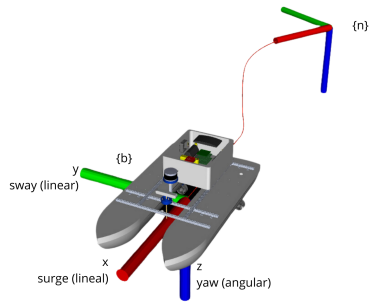


Fig. 15. Frame description for the ASV based on Fossen (2011).

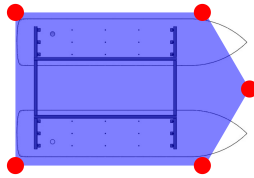


Fig. 16. Visual representation reference of the polygon enclosure for obstacle avoidance.